Proceedings of ENCIT 2008
12th Brazilian Congress of Thermal Engineering and Sciences
November 10-14, 2008, Belo Horizonte, MG

A FAST VISCOUS CORRECTION METHOD APPLIED TO THE SOLUTION OF THE EULER EQUATIONS IN TWO-DIMENSIONAL TRANSONIC FLOW

Andre Maurice Halal Lombardi, andre.maurice@gmail.com
Paulo Celso Greco Junior, pgreco@sc.usp.br
USP São Carlos, Av. Trabalhador Sancarlense, 400, São Carlos, SP, 13566-560

Roberto Gil Annes da Silva, rasilva@iae.cta.br
IAE-CTA, Praça Marechal Eduardo Gomes, 50, São José dos Campos, SP, CEP 12228-904

Abstract. *A viscous correction method is applied to the solution of the two-dimensional Euler equation. In transonic flows the interaction between shock waves and boundary layer can have large influence on the pressure distribution. The objective of the study is to improve transonic results for which shock/boundary-layer interaction is important but generates no (or very little) flow separation. The boundary-layer displacement thickness is calculated, with an integral method, using the results from the inviscid flow analysis. The calculated displacement thickness is then used to modify the lifting surface geometry and a new inviscid result is obtained. This process is repeated until convergence is achieved. The main reason for solving the Euler equation is computational cost when compared to the solution of the Navier-Stokes equations. An existing two-dimensional Euler computer code is extended to include the viscous correction. The Euler equations are approximated using the finite volume method and solved through time integration up to a steady state solution. Results for several airfoil sections are obtained. The results are compared with published experimental data and with inviscid solutions for steady transonic pressure distribution.*

Keywords: *CFD, Transonic Flow, Viscous Correction*

1. INTRODUCTION

The computer simulation of fluid flows (Computational Fluid Dynamics, CFD) came in the second half of the twentieth century with the advent of high-speed computers, making it possible to quantify the properties of the fluids without the drawbacks inherent in the experimental approach. Drawbacks such as the high cost of building the infrastructure (wind tunnels, instrumentation, models and prototypes) necessary to carry out the tests, and the difficulty of reproduction of certain flow conditions (e.g. hypersonic outlets and laminar flow). The great flexibility to simulate various types of flow on complex geometries raised CFD to the status of essential tool in many different fields, especially in aerodynamics. Its use, similar to that of other areas of simulation, is composed basically of two steps: modeling, including simplifying assumptions and derivation of governing equations, and; solving those equations, subject to the particularities of the problem in question, through an appropriate numerical method.

Many current problems stem from earlier questions in CFD, when the evaluation and simulation of the involved phenomena were poor or even non-existent. A recurrent issue is the study of dynamic aeroelasticity problems in transonic flight, dating from the end of World War II. Transonic flow (Anderson, 2003) is characterized by the presence of mixed regions (subsonic and supersonic) on the aerodynamic surfaces, with the occurrence of non-linear phenomena from the effects of compressibility, such as the formation of shock waves and their interaction with the boundary layer. Often this interaction can be neglected in the study of flutter and other aeroelastic phenomena. However, reasonably strong transonic shocks, even for small angles of attack, can have significant influence on the boundary layer. In the case of limit cycle oscillations (LCO), that interaction can not be ignored, given the potentially large amplitude of motion. Therefore, the computer simulation of these flows requires the presence of viscous effects, allowing development of the boundary layer. This can be done by adopting the Navier-Stokes equations, because they already include fluid viscosity effects in their formulation thus providing, in theory, realistic results. The solution of simplified models, such as the Euler equations (which neglects fluid viscosity), composed with corrections to account for viscous effects, represents a more economical and sufficiently accurate procedure when applied to certain cases. That is the main objective of the present work: correction of viscous effects (via calculation of compressible turbulent boundary layer) in the solution of the Euler equations for unsteady transonic flow to simulate the interaction between shock wave and boundary layer in aeroelastic phenomena such as flutter, especially in cases where there is no separated flow.

Viscous correction is implemented in an existing CFD code, Bru2D (Yagua, Basso, Azevedo, 1998), which has the capability of solving both the Reynolds Averaged Navier-Stokes (RANS) and the Euler equations for two-dimensional, unsteady, compressible flow. The viscous correction is introduced by integrating a subroutine which calculates a compressible turbulent boundary layer (method described by Sasman and Cresci, Sasman, Cresci, 1966) to the Bru2D code, so that interaction between viscous and inviscid flow is conducted by two flow variables: Mach number distribution on the aerodynamic surface and boundary layer displacement thickness. Thus, Mach number distribution is used to calculate boundary layer displacement thickness which, in turn, is used to modify the surface geometry. This change produces a new Mach number distribution and the process is repeated until convergence is reached.

2. METHODOLOGY

As mentioned before, our goal is to introduce a viscous correction method in an inviscid flow simulation code to produce acceptable results when compared to results of codes that include viscosity (involving the solution of the Navier-Stokes equations, for example). The main advantage, then, is to reduce the processing time. As a starting point, we adopted an existing computer code, the Bru2D (Yagua, Basso, Azevedo, 1998) which, although capable of simulating viscous flows, will be used to obtain the inviscid Mach number distribution on airfoil section surfaces.

2.1 Inviscid flow simulation

The unsteady two-dimensional Euler equations (Anderson, 1991) in conservative form can be written as:
Continuity

$$\frac{\partial \rho}{\partial t}+\frac{\partial (\rho u)}{\partial x}+\frac{\partial (\rho v)}{\partial y}=0 \tag{1}$$

Momentum in the x direction

$$\frac{\partial (\rho u)}{\partial t}+\frac{\partial \left(\rho u^2\right)}{\partial x}+\frac{\partial (\rho uv)}{\partial y}+\frac{\partial p}{\partial x}=0 \tag{2}$$

Momentum in the y direction

$$\frac{\partial (\rho v)}{\partial t}+\frac{\partial (\rho uv)}{\partial x}+\frac{\partial \left(\rho v^2\right)}{\partial y}+\frac{\partial p}{\partial y}=0 \tag{3}$$

Energy

$$\frac{\partial E}{\partial t}+\frac{\partial [u(E+p)]}{\partial x}+\frac{\partial [v(E+p)]}{\partial y}=0 \tag{4}$$

where u and v are, respectively, the flow velocity in the x and y directions, p is pressure, ρ is density and E is total energy, described as:

$$E=\rho\left[e+\left(\frac{u^2+v^2}{2}\right)\right] \tag{5}$$

where e is internal energy which, for ideal gases is given by:

$$e=\frac{R}{\gamma-1}T \tag{6}$$

where T is absolute temperature and γ is the specific heat ratio (1.4 for all considered cases). Therefore, given the local velocity components, u and v, local density, ρ, and total energy, E, it is possible to calculated the local temperature, T. With the local temperature it is possible to calculate the local Mach number.

Equations (1) to (4) are rewritten in compact form which allows for a more stable and direct solution procedure, especially for flows with supersonic regions, which is the case of transonic flows, present subject of study. In conservation form Eqs. (1) to (4) can be grouped into a vector of conserved variables, Q, and two vectors of convective flow, F e G:

$$Q=\begin{bmatrix}\rho\\ \rho u\\ \rho v\\ E\end{bmatrix}, \qquad F=\begin{bmatrix}\rho u\\ \rho u^2+p\\ \rho uv\\ u(E+p)\end{bmatrix}, \qquad G=\begin{bmatrix}\rho v\\ \rho vu\\ \rho v^2+p\\ v(E+p)\end{bmatrix} \tag{7}$$

With these definitions Eqs. (1) to (4) can be rewritten as:

$$\frac{\partial Q}{\partial t}=-\frac{\partial F}{\partial x}-\frac{\partial G}{\partial y} \tag{8}$$

where the desired solution comes from vector Q, in the form of flux variables. Other variables of interest, such as pressure, are calculated as a function of the flux variables. The computer code works mostly with the Q vector components, minimizing work with the primitive variables. Equation (8) can be solved through an explicit time integration procedure, lending an unsteady solution. The steady results presented here are obtained integrating the equations in time up to a steady-state condition. For each time step a new solution is calculated. Convergence to steady-state is reached when the difference between new and previous solution (on all grid points) fall bellow a specified convergence criterion. Therefore the RHS of Eq. (8) should be less than the specified convergence criterion. The equations are solved with a fifth order Runge-Kutta method (second order accurate in time) applied to an unstructured mesh composed of triangular finite volumes. Details can be found in Yagua, Basso, Azevedo, 1998.

Main parameters for running a steady simulation in Bru2D are the free flow Mach number and Reynolds number, the latter used only for density calculation in the inviscid case. Having the Mach number distribution on the airfoil surface the boundary layer displacement thickness can be calculated.

2.2 Boundary layer calculation

A conventional integral method (Sasman, Cresci, 1966) was adopted for compressible and turbulent boundary layer calculation. It is also described by Lee, 1990 implemented in the Full Potential Transonic code TAIR and, later, in the Unsteady Transonic Small Disturbance code UsTSD (Lee, 2007). In the present study the method is implemented in the solution process of the Euler equations. Prandtl equations for steady, compressible and turbulent boundary layer all variables are time averaged:

$$\frac{\partial(\rho u)}{\partial s} + \frac{\partial(\rho v)}{\partial n} = 0 \tag{9}$$

$$\rho u \frac{\partial u}{\partial s} + \rho v \frac{\partial u}{\partial n} = -\frac{dp}{ds} + \frac{\partial \tau}{\partial n} \tag{10}$$

In Eqs. (9) and (10), s represents the direction tangent to the airfoil surface, n is the normal direction, and τ is the shearing stress between the airfoil surface and the flow. Mager transformation (Mager, 1958) is employed to simplify the equations. Actually, through the transformed equations, the density variation due to the temperature gradient in the boundary layer can be described in a simpler form. The transformed equations are described by:

$$\hat{s} = \int_0^s \left(\frac{T_0}{T_{ref}}\right)\left(\frac{T_e}{T_0}\right)^{\frac{\gamma+1}{2(\gamma-1)}} ds \tag{11}$$

$$\hat{n} = \left(\frac{T_e}{T_0}\right)^{1/2} \int_0^n \frac{\rho}{\rho_0} dn \tag{12}$$

where $\hat{s}$ and $\hat{n}$ are the transformed variables. Subscripts e and 0 denote, respectively, the boundary layer edge and the stagnation properties. A reference temperature, T_{ref}, is given as a function of the Prandtl number, Pr:

$$\frac{T_{ref}}{T_0} = \frac{1}{2}\frac{T_w}{T_0} + 0.22\sqrt[3]{\mathrm{Pr}} + \left(\frac{1}{2} - 0.22\sqrt[3]{\mathrm{Pr}}\right)\left(\frac{T_e}{T_0}\right) \tag{13}$$

where T_w is the wall (airfoil surface) temperature. Adopted Prandtl number for the air flow is the standard value of 0.72. The adopted value for T_w/T_0 is unity representing adiabatic wall condition. Shape factor, H, and momentum thickness, θ, are related to the transformed shape factor, $\hat{H}$, and transformed momentum thickness, $\hat{\theta}$, by:

$$H = \left(1 - \frac{\gamma-1}{2}M_e^2\right)\hat{H} + \frac{\gamma-1}{2}M_e^2 \tag{14}$$

$$\theta = \left(\frac{T_e}{T_0}\right)^{\frac{\gamma+1}{2(\gamma-1)}} \hat{\theta} \tag{15}$$

where $H = \delta^*/\theta$, and M_e is the Mach number at the boundary layer edge which, in the present work, comes from the inviscid flow calculation. The boundary layer displacement thickness can, then, be expressed as a function of its transformed equivalent and of the transformed momentum thickness as:

$$\delta^* = \left(\hat{\theta} + \hat{\delta^*}\right)\left(\frac{T_0}{T_e}\right)^{\frac{3\gamma-1}{2(\gamma-1)}} - \left(\frac{T_0}{T_e}\right)^{\frac{\gamma+1}{2(\gamma-1)}} \hat{\theta} \tag{16}$$

The specific heat ratio, γ, was considered constant with a standard air value of 1.4. With adiabatic wall condition the transformed displacement thickness, $\hat{\delta^*}$, and transformed momentum thickness, $\hat{\theta}$, are given by:

$$\hat{\delta^*} = \int_0^{\hat{\delta}} \left(1 - \frac{\hat{U}}{\hat{U_e}}\right) d\hat{n} \tag{17}$$

$$\hat{\theta} = \int_0^{\hat{\delta}} \frac{\hat{U}}{\hat{U}_e}\left(1 - \frac{\hat{U}}{\hat{U}_e}\right) d\hat{n} \tag{18}$$

where $\hat{\delta}$ is the transformed boundary layer thickness. The transformed velocity in the s direction, $\hat{U}$, in Eqs. 17 e 18, is given by:

$$\hat{U} = u\left(\frac{T_0}{T_e}\right)^{1/2} \tag{19}$$

Using the power law for transformed velocity distribution in the boundary layer gives:

$$\frac{\hat{U}}{\hat{U}_e} = \left(\frac{\hat{n}}{\hat{\delta}}\right)^{\frac{\hat{H}_i - 1}{2}} \tag{20}$$

where $\hat{H}_i$ is the transformed adiabatic shape factor ($\hat{H}_i = \hat{\delta^*} \big/ \hat{\theta}$). Using the previous equations, it is possible to obtain the transformed integral equations:

$$\frac{d\hat{\theta}}{d\hat{s}} + \frac{\hat{\theta}}{\hat{U}_e}\frac{d\hat{U}_e}{d\hat{s}}\left(2 + \frac{T_w}{T_0}\hat{H}_i\right) = \left(\frac{T_0}{T_e}\right)^{0.268}\left(\frac{T_{ref}}{T_0}\right)^{1.268}\frac{\tau_w}{\rho_e \hat{U}_e^2} \tag{21}$$

$$\frac{d\hat{H}_i}{d\hat{s}} = -\frac{1}{2\hat{U}_e}\frac{d\hat{U}_e}{d\hat{s}}\left(\hat{H}_i + 1\right)^2\left(\hat{H}_i - 1\right) + \frac{\hat{H}_i^2 - 1}{\hat{\theta}}\left(\frac{T_{ref}}{T_e}\right)\frac{\tau_w}{\rho_e \hat{U}_e^2}\left[\hat{H}_i - \left(\hat{H}_i + 1\right)\int_0^1 \frac{\tau}{\tau_w} d\left(\frac{\hat{n}}{\hat{\delta}}\right)\right] \tag{22}$$

Equations (21) and (22) are ordinary differential equations and can be numerically integrated. However, a few modifications are still necessary to improve numerical stability and simplify their implementation. The boundary layer edge transformed velocity,$\hat{U}_e$), is replaced by the expression involving the local Mach number,M_e:

$$M_e = \frac{U_e}{a_e} = \frac{U_e}{a_0}\frac{a_0}{a_e} = \frac{U_e}{a_0}\frac{\sqrt{\gamma R T_0}}{\sqrt{\gamma R T_e}} = \frac{U_e}{a_0}\sqrt{\frac{T_0}{T_e}} \tag{23}$$

and, from Eq. (19):

$$\hat{U}_e = M_e a_0 \tag{24}$$

Equations (21) e (22) are rewritten using the boundary layer edge Mach number as the only inviscid calculation variable. The integral involving the wall shear stress, τ_w (Eq. (22)), is estimated using a semi-empirical relation:

$$\int_0^1 \frac{\tau}{\tau_w} d\left(\frac{\hat{n}}{\hat{\delta}}\right) \approx \frac{0.022}{C_f}\left(\frac{\hat{H}_i - 1}{\hat{H}_i}\right)^2 \tag{25}$$

which is applicable to both favorable and adverse pressure gradient conditions. The skin friction coefficient, C_f, is adapted for compressible flow, as:

$$C_f = 0.246 \cdot e^{-1.561\hat{H}_i}\left(\frac{T_0}{T_e}\right)^{-1}\left(\frac{T_{ref}}{T_0}\right)^{-1}\left(\frac{\mu_{ref}}{\mu_0}\right)^{0.268}\left(\frac{M_e a_0 \hat{\theta}}{\nu_0}\right)^{-0.268} \tag{26}$$

where μ_{ref} and μ_0 are the air dynamic viscosity coefficients at, respectively T_{ref} and T_0, with values which can be extracted from a standard atmosphere table. Equivalently, ν_0 is the air kinematic viscosity coefficient at T_0. The T_0/T_e ratio is described by:

$$\frac{T_0}{T_e} = 1 + \frac{\gamma - 1}{2}M_e^2 \tag{27}$$

A new variable is defined:

$$f = \left(\frac{\hat{U}_e \hat{\theta}}{\nu_0}\right)^{1.268} = \left(\frac{M_e a_0 \hat{\theta}}{\nu_0}\right)^{1.268} \tag{28}$$

to eliminate the singularity in Eq. (21) for $\hat{\theta} = 0$. Using Eqs. (24) to (28), the final form of the integral equations is obtained:

$$\frac{df}{ds} = 1.268\left[A - \frac{f}{M_e}\frac{dM_e}{ds}\left(2 + \hat{H}_i\right)\right] \tag{29}$$

$$\frac{d\hat{H}_i}{ds} = A\frac{\hat{H}_i^2 - 1}{f}\left[\hat{H}_i + \frac{0.022\,T_0}{C_f\,T_{ref}}\left(\hat{H}_i + 1\right)\left(\frac{\hat{H}_i - 1}{\hat{H}_i}\right)^2\right] - \frac{\left(\hat{H}_i - 1\right)\left(\hat{H}_i + 1\right)^2}{2M_e}\frac{dM_e}{ds} \tag{30}$$

where A is given by:

$$A = 0.123e^{-1.561\hat{H}_i}\left(\frac{M_e a_0}{\nu_0}\right)\left(\frac{T_e}{T_{ref}}\right)\left(\frac{T_e}{T_0}\right)^3\left(\frac{\mu_{ref}}{\mu_0}\right)^{0.268} \tag{31}$$

Both Eqs. (29) and (30) have the influence of Mach number distribution at the boundary layer edge, M_e. That is the mechanism which will transmit information from the inviscid calculation to the boundary layer. Information is then sent back to the inviscid flow through the boundary layer displacement thickness which is used to modify the airfoil geometry.

Numerical solution of Eqs. (29) and (30) is carried out using a hybrid fourth and fifth order Runge-Kutta method. Adopted initial conditions for all cases are $H_i = 1.7$ and $\theta = 0$. The second condition still produces singularity in Eq. (30) and, in the first integration step, the value of H_i is kept constant. For the following steps θ is no longer null and H_i can be normally calculated. The first initial condition, $H_i = 1.7$, is a typical reference value for turbulent flow and rapidly converges to values consistent with the solution of Eqs. (29) and (30).

The result sent back to the inviscid flow calculation is the displacement thickness, δ^*, which is used to modify the airfoil geometry. The modification consists of simply adding δ^* to the airfoil thickness (normal to the surface). Therefore, the solution starts with the original airfoil section and ends up with a thicker, new airfoil geometry reproducing the boundary layer effect on the inviscid flow. The displacement thickness is calculated using Eq. (16) considering that $\hat{H}_i = \hat{\delta^*}/\hat{\theta}$ (where $\hat{H}_i$ e $\hat{\theta}$, the latter obtained from Eq. (28), are the solutions of Eqs. (29) and (30)). The new inviscid solution is used to calculate the boundary layer again. This process is repeated until convergence to steady state is achieved.

The simulation is limited to cases with no (or very little) flow separation restricting simulation to small angles of attack. It is assumed that the boundary layer is totally turbulent, reasonable for transonic high Reynolds flow where the laminar region is very small. Prediction of transonic flutter at low angle of attack would be a viable application since the stability analysis use small perturbations. Better prediction of shock intensity and position, with little added computational cost, is a potential advantage of the presented method.

3. RESULTS

Initially, inviscid simulations were conducted, with the Bru2D code, for several Mach number and angle of attack conditions. The computational meshes were generated using the commercial software ANSYS ICEM CFD and consist of unstructured meshes with triangular elements in a circular domain. The use of sub grid regions allowed for better refinement control. Figure 1 shows an example of mesh for the NACA 0012 airfoil section.

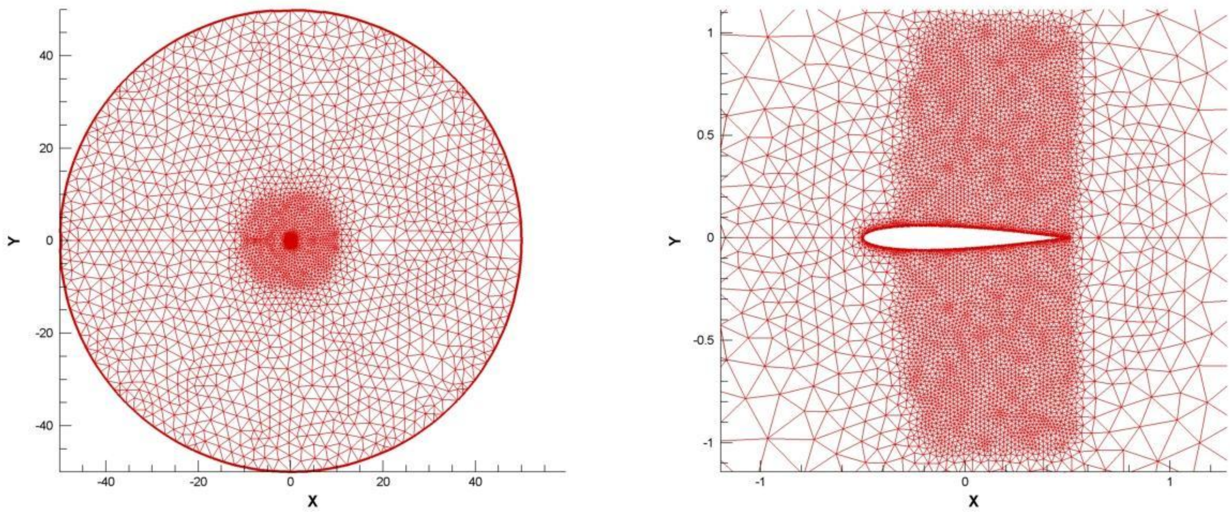

Figure 1. General view of the computational mesh (unstructured) generated for the NACA 0012 airfoil section (left), and enlarged airfoil region showing refinement details in the shock wave region (right).

After convergence to steady state the Mach number distribution on the airfoil surface were loaded in the viscous correction routine and a boundary layer displacement thickness distribution was obtained. Free stream properties were adjusted to produce a specified Reynolds number, typically between 5 and 8 million for transonic wind tunnel tests.

Under those conditions the flow around a NACA 0012 airfoil section (Fig. 2) was simulated for a few angles of attack (small), leading to stable solutions for the boundary layer integration procedure.

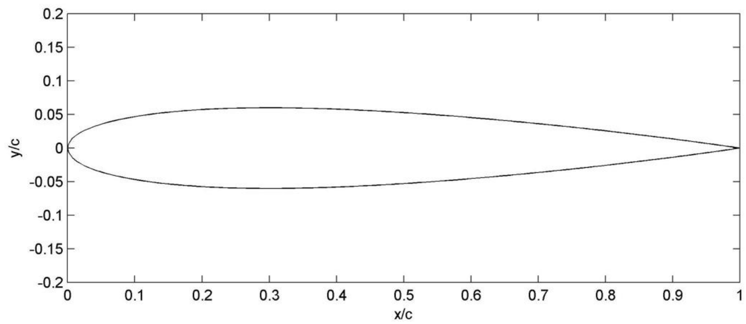

Figure 2. NACA 0012 airfoil section.

Figure 3 shows the Mach number distribution on the upper surface of the NACA 0012 airfoil for angle of attack,α, equal to 0^o and free stream Mach number, M_∞, equal to 0.755. A shock wave (characterized by the abrupt decrease from supersonic to subsonic) is formed around $x/c = 0.3$. This Mach number distribution was used to calculate the boundary layer displacement thickness shown in Fig. 4. Reynolds number, Re, is 5.3 million.

Figure 4 shows a slight increase in displacement thickness coinciding with the shock position around $x/c = 0.3$, as seen in Fig. 3. Figure 5 shows the pressure coefficient distribution on the airfoil upper surface, calculated by Bru2D (black marks) and from experimental data (Thibert, Ohman, 1979, red marks).

The inviscid numerical results overestimate the shock wave intensity for this result without viscous correction. The effect of the boundary layer, when introduced, should be of pushing the shock wave upstream and reducing its intensity, improving the correlation with the experimental results. A secondary effect of the viscous correction is the exponential like thickening at the trailing edge which is also likely to modify the corrected pressure distribution. Only the upper surface results are shown since the case should be symmetrical. Actually there is a small asymmetry between upper and lower surfaces due to an asymmetry of the unstructured mesh.

Figures 6, 7 e 8 show the results, no viscous correction, with $M_\infty = 0.8$ and $\alpha = 0°$. For this condition the shock wave is stronger than that for $M_\infty = 0.755$. This increase in shock intensity is followed by a larger increase in displacement thickness on the shock location. It can be noted in Fig. 4 that, immediately downstream of the shock position, there is a reduction in δ^* indicating restitution of boundary layer. This behavior is consistent with that observed in Fig. 5 which shows a slight favorable pressure gradient after the shock.

Through an initial implementation of the viscous correction in the Bru2D code, preliminary results for steady-state condition were obtained, as shown in Figures 9 through 13. These results were acquired by introducing only a percent of the boundary layer displacement thickness into the airfoil surface and, then, allowing the inviscid code (Bru2D) to cope with the change in geometry during a few iterations. After an acceptable residue (RHS in Equation 8) is obtained, the initial percent is increased and the (recalculated) boundary layer displacement thickness is reintroduced, and this process is conducted until it is fully inserted. However, due to some instabilities pertaining to both Bru2D code and viscous correction routine, sometimes it was not possible to reach convergence when 100% of the boundary layer displacement thickness was introduced. In this case, convergence can be reached only for lesser percents.

Figure 9 shows the Mach number distribution on the upper surface of the NACA 0012 airfoil for angle of attack, α, equal to 0^o and free stream Mach number, M_∞, equal to 0.755. Comparing with the inviscid result, it can be seen that the shock was moved upstream and had its intensity slightly reduced. The same can be observed from Figure 10, where experimental results for the same condition are shown. Figure 11 shows the boundary layer displacement thickness calculated for this case. As expected, at approximately 30% of the chord, which corresponds to the shock position, there is a slight increase in the boundary layer displacement thickness. These results were obtained by introducing 85% of the boundary layer displacement thickness, although some noise can be seen immediately after the shock and at the trailing edge.

Figures 12 through 13 show the results obtained for NACA 0012 airfoil for angle of attack, α, equal to 0^o and free stream Mach number, M_∞, equal to 0.829. Although only 45% of the total boundary layer was inserted, the increase in the free stream Mach number caused a more intensive shock and also larger oscillations after the shock and at the trailing edge. Nevertheless, the effect of the viscous correction, depicted by the new position of the shock upstream (better showed by Figure 13), still can be observed.

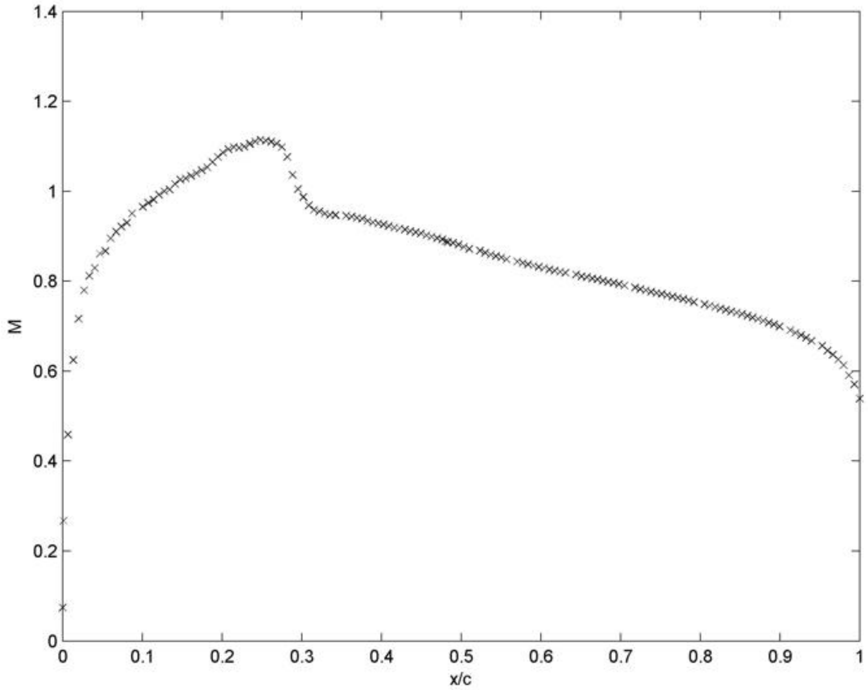

Figure 3. Mach number distribution on the upper surface of the NACA 0012 airfoil. Inviscid simulation (no viscous correction) from Bru2D code with $M_\infty = 0.755$ and $\alpha = 0°$.

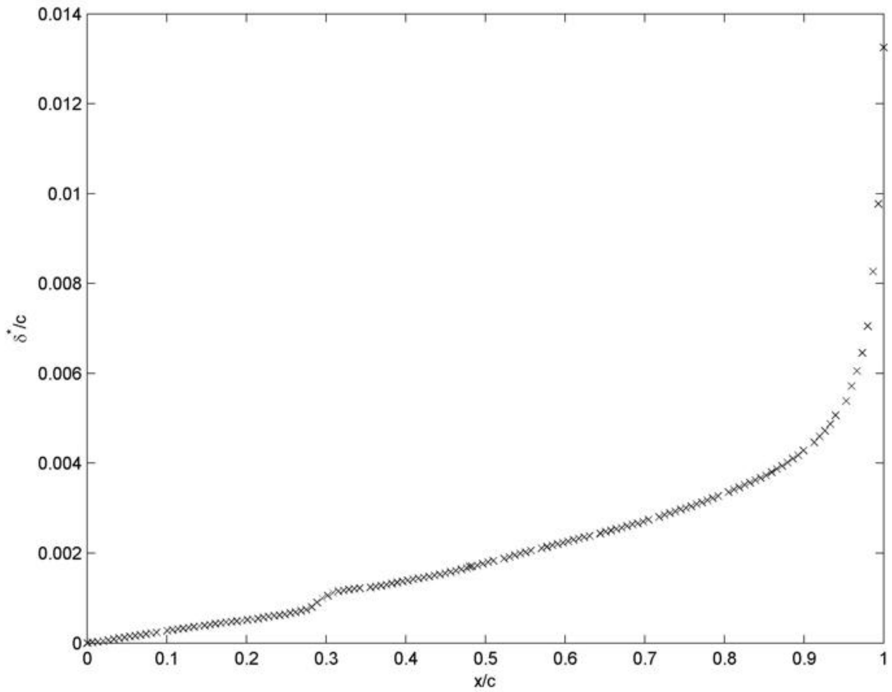

Figure 4. Boundary layer displacement thickness on the upper surface of the NACA 0012 airfoil. Simulation with $M_\infty = 0.755$, $\alpha = 0°$ and $Re = 5.3 \times 10^6$.

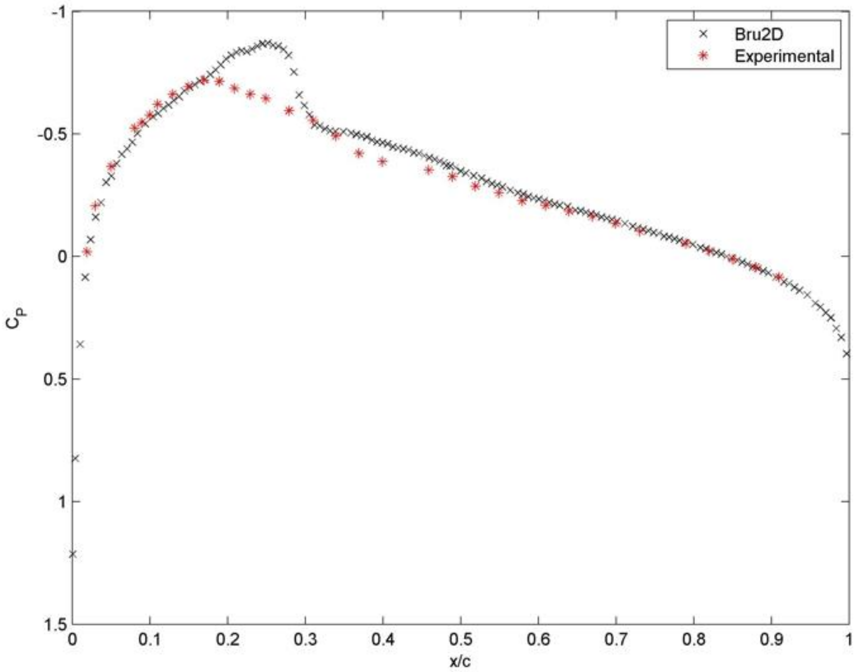

Figure 5. Pressure coefficient distribution on the upper surface of the NACA 0012 airfoil. Inviscid simulation (no viscous correction) from Bru2D code with $M_\infty = 0.755$ and $\alpha = 0°$ and comparison with experimental results (Thibert, Ohman, 1979).

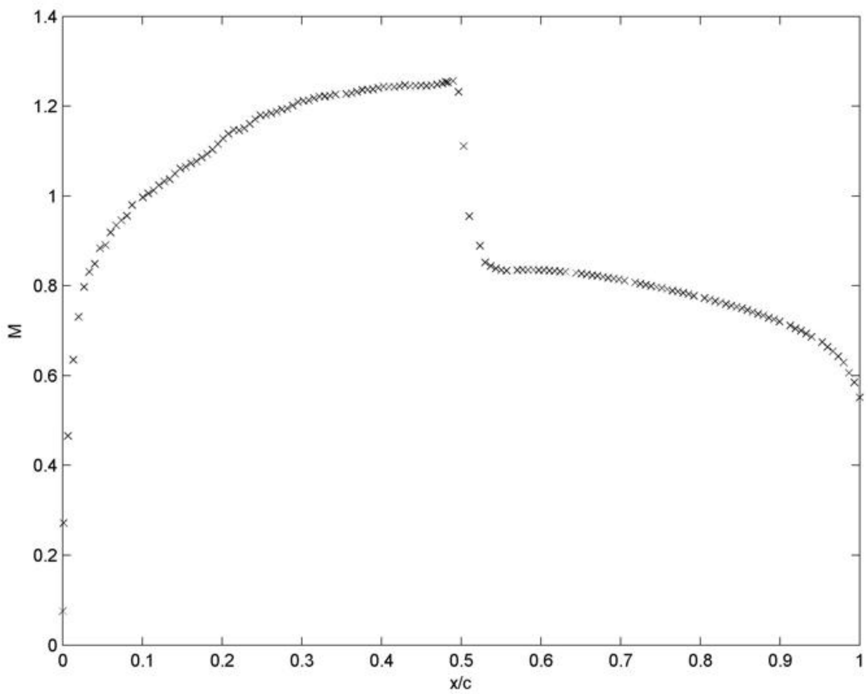

Figure 6. Mach number distribution on the upper surface of the NACA 0012 airfoil. Inviscid simulation (no viscous correction) from Bru2D code with $M_\infty = 0.8$ and $\alpha = 0°$.

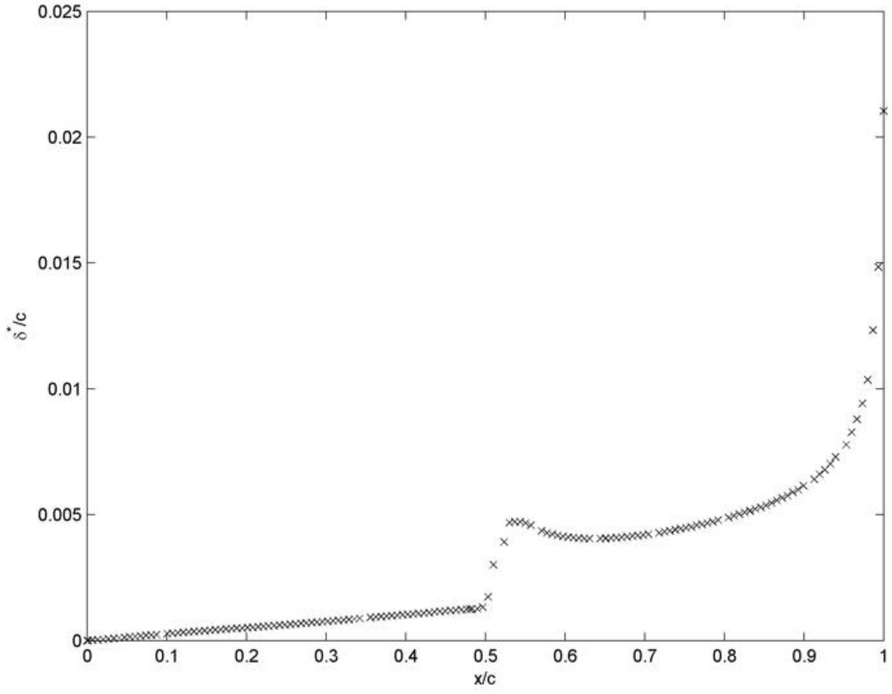

Figure 7. Boundary layer displacement thickness on the upper surface of the NACA 0012 airfoil. Simulation with $M_\infty = 0.8$, $\alpha = 0°$ and $Re = 5.3 \times 10^6$.

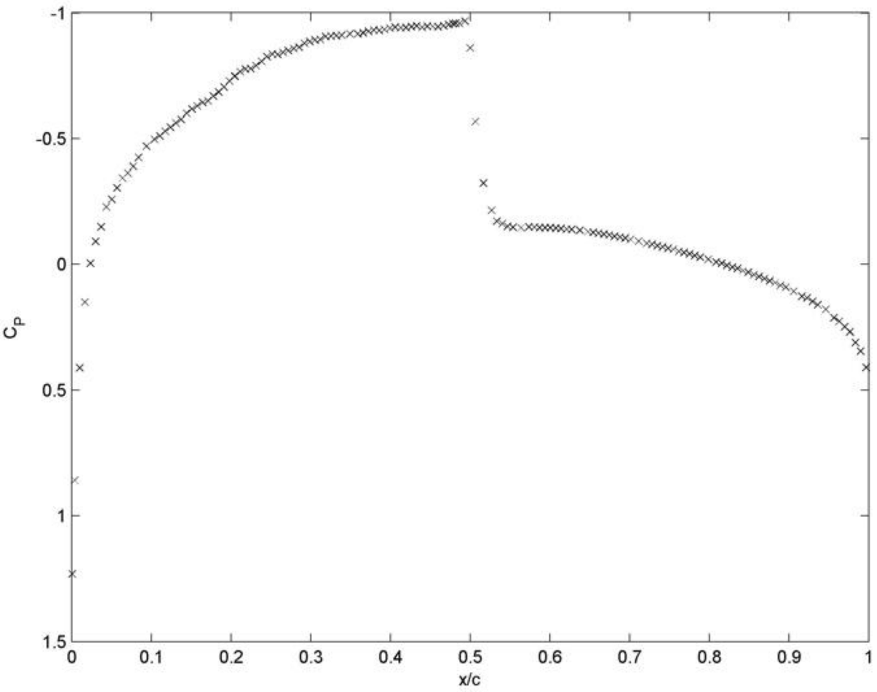

Figure 8. Pressure coefficient distribution on the upper surface of the NACA 0012 airfoil. Inviscid simulation (no viscous correction) from Bru2D code with $M_\infty = 0.8$ and $\alpha = 0°$.

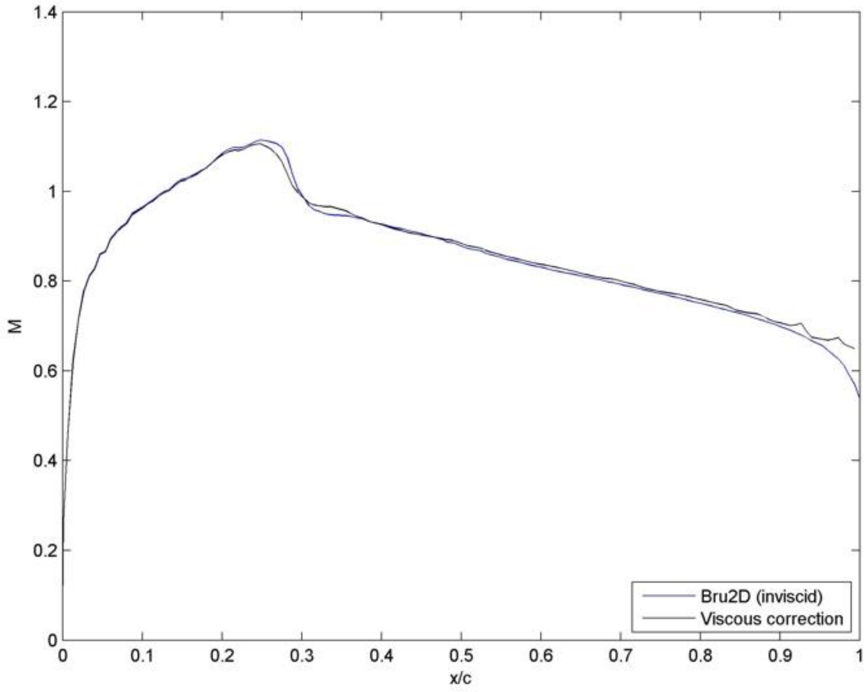

Figure 9. Mach number distribution on the upper surface of the NACA 0012 airfoil. Inviscid simulation from Bru2D code and results obtained from the viscous correction with $M_\infty = 0.755$ and $\alpha = 0°$.

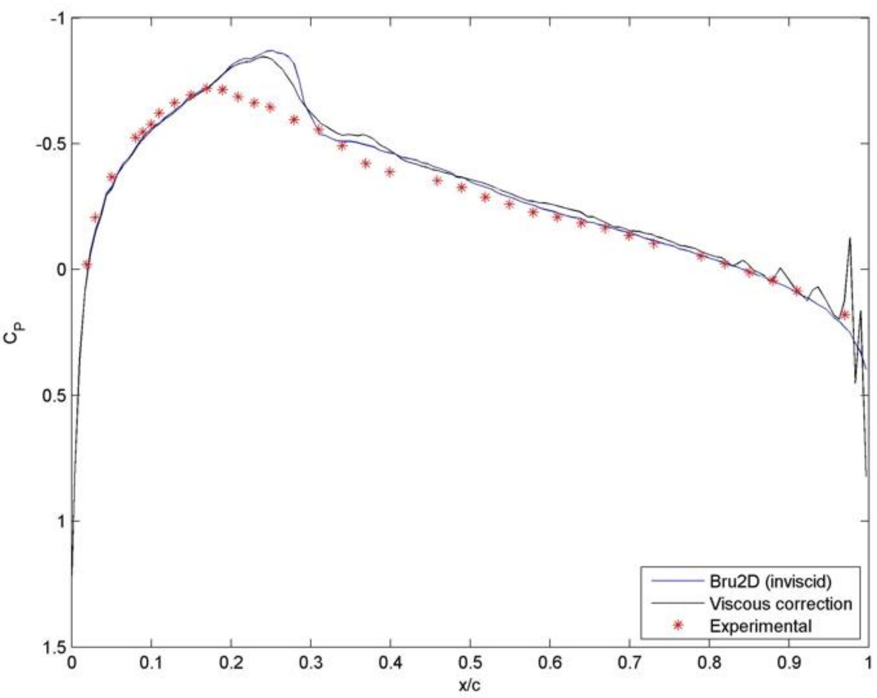

Figure 10. Pressure coefficient distribution on the upper surface of the NACA 0012 airfoil. Inviscid simulation from Bru2D code and results obtained from the viscous correction with $M_\infty = 0.755$ and $\alpha = 0°$ and comparison with experimental results (Thibert, Ohman, 1979).

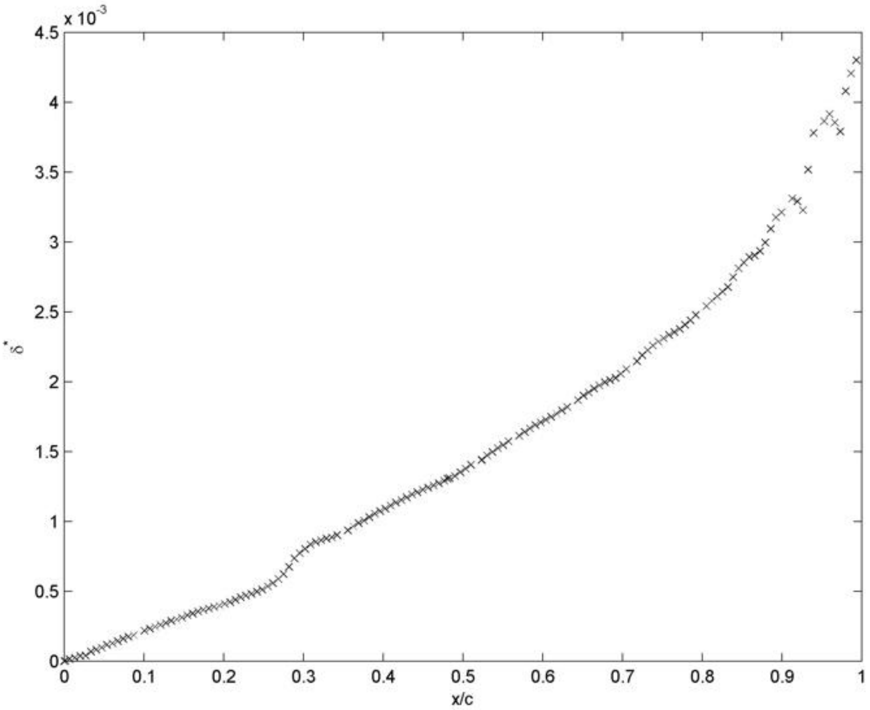

Figure 11. Boundary layer displacement thickness on the upper surface of the NACA 0012 airfoil. Simulation with $M_\infty = 0.755$, $\alpha = 0°$ and $Re = 5.3 \times 10^6$.

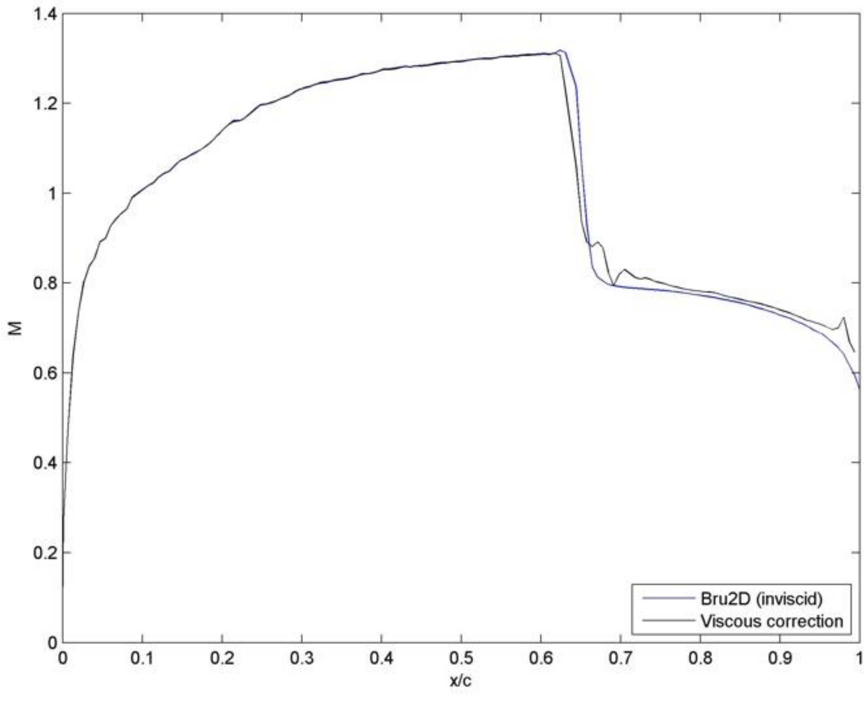

Figure 12. Mach number distribution on the upper surface of the NACA 0012 airfoil. Inviscid simulation from Bru2D code and results obtained from the viscous correction with $M_\infty = 0.755$ and $\alpha = 0°$.

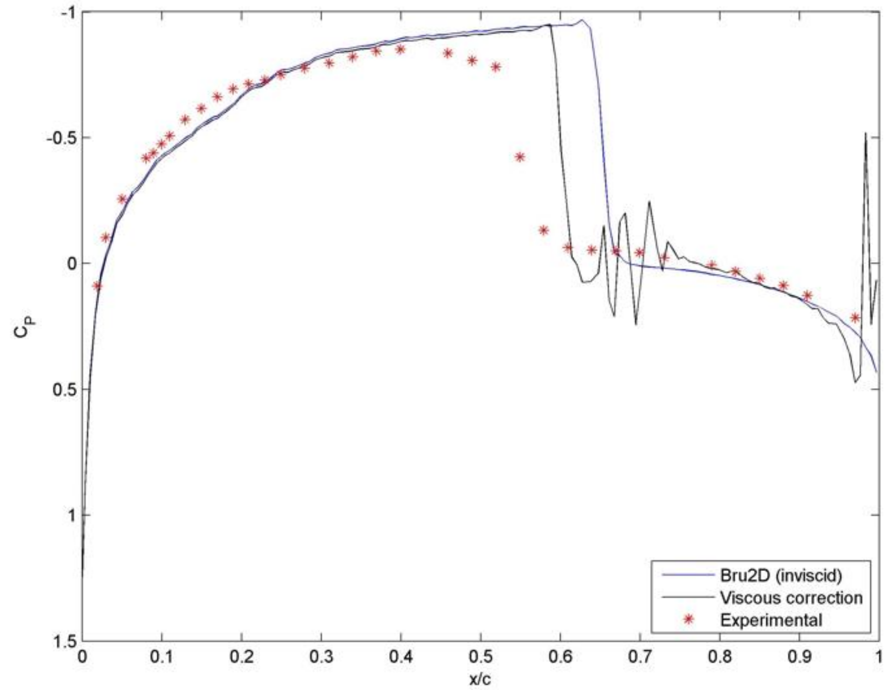

Figure 13. Pressure coefficient distribution on the upper surface of the NACA 0012 airfoil. Inviscid simulation from Bru2D code and results obtained from the viscous correction with $M_\infty = 0.755$ and $\alpha = 0°$ and comparison with experimental results (Thibert, Ohman, 1979).

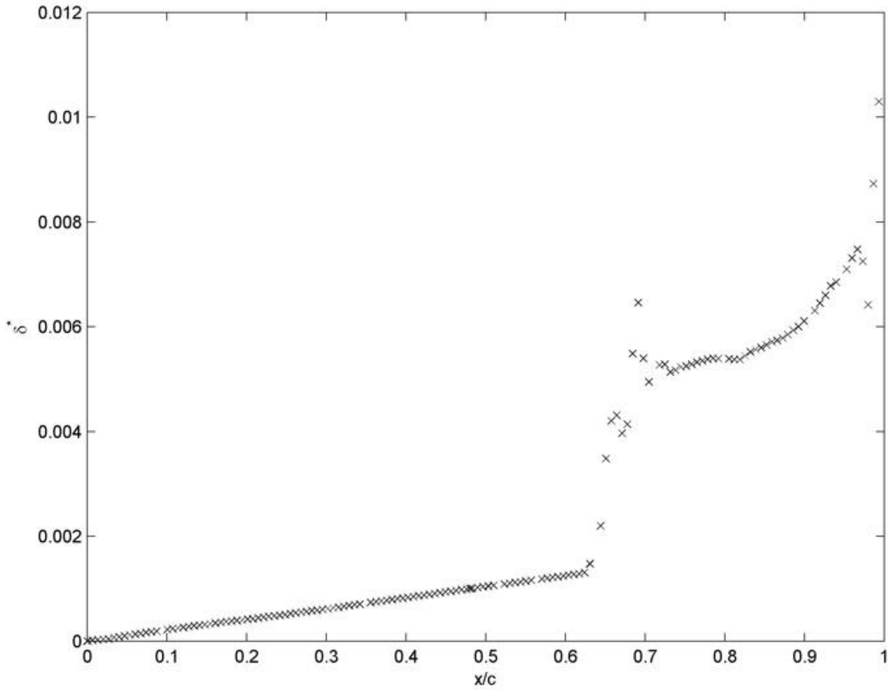

Figure 14. Boundary layer displacement thickness on the upper surface of the NACA 0012 airfoil. Simulation with $M_\infty = 0.755$, $\alpha = 0°$ and $Re = 5.3 \times 10^6$.

4. CONCLUSION

The present work describes a method for viscous correction of the Euler equations. Simulation of viscous flows using the Navier-Stokes equations usually have much higher computational cost than inviscid models. Solving the Euler equations with viscous corrections can potentially generate good results, within limits of application, with lower cost. The results show good potential for solving two-dimensional, low angle of attack, transonic cases in which shock/boundary-layer is significant but there is little or no flow separation.

Application of the described method will be extended to unsteady cases in which the boundary layer will be updated at each time step. It will also be extended to three-dimensional cases using a stream wise two-dimensional approximation for the boundary layer. The main final objective is to reach a good methodology for low cost transonic flutter analysis of three dimensional configurations.

5. ACKNOWLEDGEMENTS

The authors wish to thank FAPESP for financing the present work trough grants 2007/06573-1 and 2004/16064-9.

6. REFERENCES

Anderson, J. D., 1991, *Fundamentals of Aerodynamics*, 2nd edition, McGraw-Hill.

Anderson, J. D., 2003, *Modern Compressible Flow*, 3rd edition, McGraw-Hill.

Lee, S. C., 1990, "A Fast Viscous Correction Method for Transonic Aerodynamics", *Computational Methods in Viscous Aerodynamics*, Chapter 10, T.K.S. Murthy and C.A. Brebbia editors, Elsevier.

Lee, Y. S., 2007, *Correção de Efeitos Viscosos na Solução do Escoamento Potencial de Pequenas Perturbações em Regime Transônico no Domínio da Frequência*, 95 f. Tese (Doutorado), Escola de Engenharia de São Carlos, Universidade de São Paulo, São Paulo.

Mager, A., 1958, "Transformation of the Compressible Turbulent Boundary Layer", *Journal of Aerospace Science*, Vol. 25, No. 5, pp. 305-311.

Sasman, P. K., Cresci, R. J., 1966, "Compressible Turbulent Boundary Layer with Pressure Gradient and Heat Transfer", *AIAA Journal*, Vol. 4, No. 1, pp. 19-25.

Thibert, J. J., Ohman, L. L., 1979, "NACA 0012 Airfoil - Pressure Distribution, and Boundary Layer and Wake Measurements", *AGARD AR-138-Experimental data base for computer program assessment*.

Yagua, L. C. Q., Basso, E., Azevedo, J. L. F., 1998, "Esquemas de Malhas Sobrepostas para as Equações de Euler Bidimensionais em Escoamentos Compressíveis", *Anais do VII Congresso Brasileiro de Engenharia e Ciências Térmicas*, Rio de Janeiro, RJ, ABCM, Vol. 1, pp. 1-6.

7. Responsibility notice